

Article

Surface Plasmon Resonance Sensor Based on Polypyrrole–Chitosan–BaFe₂O₄ Nanocomposite Layer to Detect the Sugar

Amir Reza Sadrolhosseini ^{1,*}, Pooria Moozarm Nia ², Mahmoud Naseri ³,
Ahmad Mohammadi ⁴, Yap Wing Fen ^{5,*}, Suhidi Shafie ¹ and Halimah Mohamed Kamari ⁵

¹ Functional Device Laboratory, Institute of Advanced Technology, Universiti Putra Malaysia (UPM), Selangor 43400, Malaysia; suhaidi@upm.edu.my

² Advance Material Research Group, Center of Hydrogen Energy, Institute of Future Energy, Universiti Technology Malaysia, Kuala Lumpur 58000, Malaysia; pooriamn@yahoo.com

³ Department of Physics, Faculty of Science, Malayer University, Malayer 65719-95863, Iran; mahmoud.naseri55@gmail.com

⁴ Department of Electrical and computer Engineering, Buein Zahra Technical University, Buein Zahra, Qazvin 34517-45346, Iran; mohamadi@bzte.ac.ir

⁵ Department of Physics, Faculty of Science, Universiti Putra Malaysia (UPM), Selangor 43400, Malaysia; halimahmk@upm.edu.my

* Correspondence: amir.reza@upm.edu.my (A.R.S.); yapwingfen@gmail.com (Y.W.F.); Tel.: +601-3319-0104 (A.R.S.); +601-2819-093 (Y.W.F.)

Received: 22 August 2019; Accepted: 30 September 2019; Published: 20 April 2020



Abstract: The surface plasmon resonance sensor was used to detect and measure low concentrations of sugar. A polypyrrole–chitosan–BaFe₂O₄ nanocomposite layer was prepared to improve the surface of the gold layer for the detection of glucose, fructose, and sucrose using the surface plasmon resonance technique. The polypyrrole–chitosan–BaFe₂O₄ was synthesized using the electrodeposition method in different thicknesses. The functional group, crystal structure, and morphology of the layer were investigated with Fourier transform infrared spectroscopy, X-ray diffraction technique, and field emission electron microscopy. Consequently, the BaFe₂O₄ was scattered on the surface of the polymer, and the affinity of polypyrrole–chitosan–BaFe₂O₄ to bond with glucose is higher than that for the other sugars. The sensor limit was 0.005 ppm.

Keywords: surface plasmon resonance; BaFe₂O₄; polypyrrole; chitosan; sugar

1. Introduction

In the last decade, many researchers focused on the detection and measurement of the low concentration of sugar such as glucose, fructose, and sucrose [1]. Sugars are found in the blood, food, and beverages. Numerous methods have been used to measure glucose, fructose, and sucrose levels, including colorimetric [2], infrared [3], Raman [4], and electrochemistry spectroscopy [5]. Other analytical methods such as gas chromatography and mass spectroscopy were considered to investigate sugar levels in human and natural products with a limit in the range of mM to μM [6]. The optical method is an interesting technique to evaluate chemical and biochemical properties [7]. Hence, the detection and measurement of low concentrations of glucose, fructose, and sucrose were carried out using a laser interferometer [8] Ultraviolet-visible (UV-Vis) absorption spectroscopy, fluorescence spectroscopy, the optical polarization properties of medium and heterodyne polarimetry [9,10], reflected THz radiation [11], and a surface plasmon resonance sensor [12–14]. Recently, glucose biosensors have been presented based on enzymatic catalysts in three versions of enzymatic glucose biosensors [15].

The limitation of these sugar biosensors depends on the performance of these sensors—that is, the inherent instability [16] and the sensitivity of these type of biosensors depends on pH, the temperature of samples, and concentration of oxygen [17,18].

The ratio of signal to noise and immobilization of sugar to the sensing layer are the significant parameters to design the application of glucose, fructose, and sucrose sensors [19,20]. Therefore, the nanoparticles (Au, Ag, Fe₂O₃, and ZnO) and conductive polymer (polypyrrole) were used to increase and improve the ratio of signal to noise and immobilization in sugar sensors. Polypyrrole has the potential of electron transfer, because the electron transfer between sugar and the sensing layer is slow [1]. Hence, the coupling of nanoparticles and polypyrrole can improve the electron transfer in the procedure of sugar detection (sensor) [1,16], and it can also enhance the selectivity and sensitivity of the sensor.

Moreover, the surface plasmon resonance (SPR) sensor is a versatile and accurate method to detect the chemical materials and sugars. The SPR phenomenon occurs at the interface of two mediums with opposite dielectric signs. Normally, the gold layer is used for the SPR sensors, and the sensing layer has been coated on the surface of the gold layer to improve the sensitivity and selectivity of the sensor. Recently, the nanocomposite layers have been used for the sensing layer. The gold nanoparticle, carbon-based nanostructure [1], and magnetic nanoparticles were used to improve the sensitivity of the sugar sensor. Magnetic nanoparticles have some advantages, such as high catalytic efficiency, good stability, and monodispersion [2]. Hence, many researchers used the magnetic nanoparticles such as ZnFe₂O₄ [2], Fe₃O₄ [21], and polypyrrole–chitosan/Fe₂O₃ nanocomposite [16] to detect glucose and other sugars; the detection limit was in the range of 1 to 3 μM, and the ratio of signal to noise was about 3. Consequently, the magnetic nanoparticles are a considerable nanostructure to design the sugar sensor.

In this study, a polypyrrole–chitosan–BaFe₂O₄ (PPy–Chi–BaFe₂O₄) nanocomposite layer was prepared using the electrochemical method. The prepared layer was characterized using the field emission scanning electron microscopy (FE-SEM), the X-ray diffraction (XRD), and the Fourier transform infrared spectroscopy (FT-IR). The characterized layer was used to detect the glucose, fructose, and sucrose using the surface plasmon resonance technique.

2. Materials and Methods

2.1. Materials

To prepare the PPy–Chi–BaFe₂O₄, commercial chemical components were used. Iron nitrate (Fe(NO₃)₃·9H₂O) and barium nitrate (Ca(NO₃)₂·6H₂O), polyvinyl alcohol (PVA, MW = 31,000 g/mol), glucose, sucrose, fructose, chitosan (medium molecular weight (75–85% deacetylated), lithium perchlorate, and potassium dihydrogen phosphate were purchased from Sigma Aldrich company. The materials were in high quality, and had high purity of about 99%. The saturated calomel electrodes (SCE) was used as a reference electrode from BASi Company.

2.2. Preparation of Polypyrrole–Chitosan–BaFe₂O₄

2.2.1. Synthesis of BaFe₂O₄

To synthesize the PPy–Chi–BaFe₂O₄ nanocomposite layer, a PVA/BaFe₂O₄ nanocomposite was prepared using the thermal treatment method [22–24]. Ba(NO₃)₂·H₂O, Fe(NO₃)₃·H₂O, DDW, and polyvinyl alcohol (PVA) were used to precursors, solvent, and capping agent, respectively [24].

First, 3.5 g of PVA was dissolved in 100 mL of DDW at 353 K. After that, 0.2 mmol Fe(NO₃)₃·H₂O and 0.1 mmol Ca(NO₃)₂·H₂O (Fe:Ba=2:1) were added into the PVA solution, and the mixture was stirred constantly for 1.5 h, and a clear solution was obtained. The clear mixture was heated at 362 K for 24 h to remove the solvent (deionized distilled water, or DDW), and the solid BaFe₂O₄ was reminded. The product was grounded in a mortar to obtain the uniform powder, and it was heated at 773 K for

crystallization of the nanocrystal and decomposition of the PVA. The final powder was used to prepare the PPy–Chi–BaFe₂O₄.

2.2.2. Synthesis of PPy–Chi–BaFe₂O₄ Composite Layer

The PPy–Chi–BaFe₂O₄ was synthesized using the electrodeposition method. The gold-coated glass slide was prepared using a sputtering coating method, and the pyrrole was polymerized on the surface of the gold layer in the presence of chitosan and BaFe₂O₄ using the cyclic voltammetry method.

To prepare the electrolyte solution for the electrodeposition of PPy–Chi–BaFe₂O₄, 0.2 g of chitosan powder was dissolved in 50 ml aqueous solution of 0.3M oxalic acid, and it was stirred 4 h prior to its use for the preparation of the layer. The monomer solution contains mixed electrolytes in a 0.1 M phosphate buffer solution (pH 7.2), 0.1 M pyrrole monomer, 0.1 M LiClO₄ as a dopant, 0.1 M chitosan, and 0.05 g of BaFe₂O₄. The electrolyte was stirred during electrodeposition to make sure there is no precipitation. The working electrode, reference electrode, and counter electrode were a gold-coated glass slide, saturated calomel electrodes (SCE), and platinum electrode, respectively. The polymerization of pyrrole was carried out at the potential range of 0 V to 0.8 V in the presence of chitosan and BaFe₂O₄ nanoparticles at different cycles from 1 to 50. The prepared samples were put in the oven for 2 h to dry the layers. The PPy–Chi–BaFe₂O₄ composite layers were characterized using the FT-IR spectrometer (model: NEXUS), XRD spectrometer (WITec, Alpha 300R with Shimadzu diffractometer: model XRD6000 and Cu, Ka (0.154 nm)), and the FE-SEM (NOVA NANOSEM 230)

2.3. Surface Plasmon Resonance Setup

The SPR setup based on the Kretschmann configuration was used to measure the low concentration of glucose, fructose, and sucrose. Figure 1 shows the SPR setup with a high index prism based on angular modulation, and the variation of laser beam intensity was detected at a different angle using a silicon photodetector.

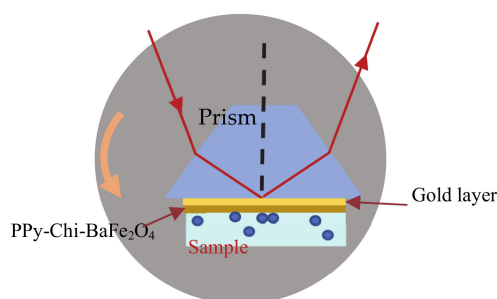


Figure 1. The surface plasmon resonance (SPR) setup to test the PPy–Chi–BaFe₂O₄ sensing layer .

The PPy–Chi–BaFe₂O₄ composite layer was deposited on the gold side of the glass slide, and it was attached to a high index prism (SF52, Focetek) using the index matching gel (F-IMF-105, Newport, USA) [12,24,25]. The prism was placed on a precision rotation stage, and the fluid holder was contacted to the sensing layer using an O-ring. The glucose, fructose, and sucrose were contacted separately to the sensing layer. The rotation stage was rotated up to 14° at increments of 0.01°. The intensity of the laser beam and the angle of rotation were registered when the rotation stage was stopped momentarily.

The experiment was repeated separately for each sugar about 10 times. The SPR signal was analyzed using the Fresnel's theory based on the matrix method for a multi-layer system [26].

2.4. Preparation of Sugar Solution

First, 0.1 g of glucose, sucrose, and fructose were separately used to prepare the high concentration of sugar solution in 100 ml of the deionized distilled water (DDW). Other concentrations of the sugar solution, including 0.005 ppm (0.0005 mg/dL), 0.05 ppm (0.005 mg/dL), 0.5 ppm (0.05 mg/dL), 5 ppm

(0.5 mg/dL), 15 ppm (1.5 mg/dL), and 25 ppm (2.5 mg/dL), were systematically prepared by dissolving the sugars solution in the DDW.

In this research, glucose, fructose, and sucrose (three sugars) in six concentrations were used to do the experiment, and the SPR experiment was repeated 10 times for each concentration of sugar.

3. Results and Discussion

Figure 2 shows the FT-IR spectrum, XRD analysis result, and FE-SEM image. Figure 2a shows the FT-IR spectrum; the main peaks of the FT-IR spectrum appeared at 3257.85, 2930.02, 1630.1, 1525.39, 1428.81, 1283.03, 1021.22, 964.53, 673.36, and 617.05 cm^{-1} . The peaks at 3257.85, 1525.39, and 1428.81 cm^{-1} related to the stretching vibrations of N–H, C–N, and C–C in the pyrrole ring, respectively [27,28]. The peak centered at 2930.02 cm^{-1} corresponded to the asymmetric vibration of CH_2 , and the peaks that appeared at 1283.03, 1021.22, and 964.53 cm^{-1} were assigned to the C–H deformation, C–O–C, and the C–N stretching vibration of PPy, respectively. Moreover, the peaks located at 3257.85 and 2930.02 cm^{-1} corresponded to N–H, while the vibration of CH_2 of the chitosan chain overlapped on the vibration of N=H and CH_2 in polypyrrole [28]. The peaks at 1630.1, 673.36, and 617.05 cm^{-1} presented a vibration of C=O in the amid band, N–H out of the plane, and O–H out of the plane in chitosan [29].

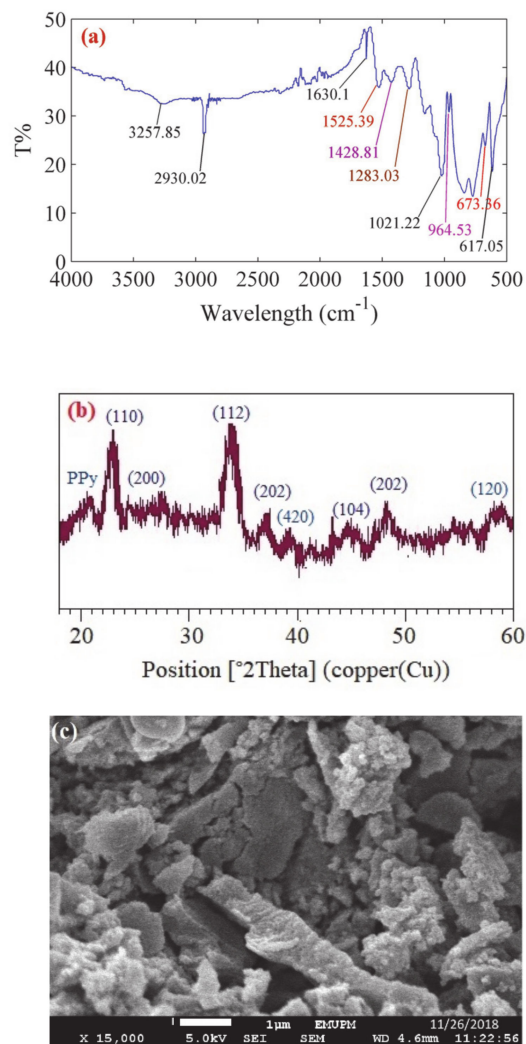


Figure 2. (a) The Fourier transform infrared spectroscopy (FT-IR) spectrum, (b) XRD result, and (c) FE-SEM image.

Figure 2b shows the XRD spectrum of the PPy–Chi–BaFe₂O₄ nanocomposite layer. Following the literature, the XRD spectrum of PPy–Chi appears at 21.4° [29], which explains the PPy–Chi that formed in the amorphous form in the thin layer. The main peak of the XRD spectrum for BaFe₂O₄ appeared at 23.3°, 24.4°, 34.23°, 37.1°, 39.5°, 45.2°, 48.1°, and 59.7°, which related to reflection plane of (110), (200), (112), (202), (420), (104), (202), and (120), respectively. They confirm that BaFe₂O₄ has a face-centered cubic structure [30]. The XRD pattern of PPy–Chi–BaFe₂O₄ confirms that the BaFe₂O₄ also formed in the composite layer in the cubic structure. During the electrodeposition process, monomer molecules and metal ions at the electrode–electrolyte interface deposited on the surface of the working electrode by reaching the proper applied potential, and the mechanism is as follows [28]:

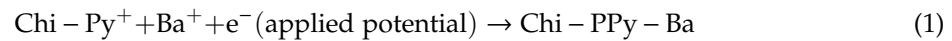


Figure 2 shows the FE-SEM image of the PPy–Chi–BaFe₂O₄ nanocomposite layer. The PPy–Chi–BaFe₂O₄ composite layer was formed during electro-polymerization of pyrrole in the presence of chitosan, LiClO₄ (as a dopant), and BaFe₂O₄ nanoparticles, and the chitosan agglomerated the polypyrrole and BaFe₂O₄ nanoparticles during the electro-polymerization of pyrrole. Finally, the PPy–Chi–BaFe₂O₄ composite layer was formed on the surface of the gold layer [16]. BaFe₂O₄ nanoparticles (NPs) were scattered on the surface of layer, and it impressed the morphology of the PPy–Chi–BaFe₂O₄ nanocomposite layer [31].

The essential charges for organizing the PPy were the electrons and anions that LiClO₄ and BaFe₂O₄ provided them. Therefore, the role of LiClO₄ and BaFe₂O₄ were as the electron and anions charges to create the counterbalance of the PPy–Chi–BaFe₂O₄ composite layer. Hence, the polymer electropolymerized at the surface of the working electrode, containing BaFe₂O₄ nanoparticles [32].

The gold/PPy–Chi–BaFe₂O₄ system layer was prepared in different thickness. The thickness of the gold layer was 48.3 nm, and the thickness of the PPy–Chi–BaFe₂O₄ composite layers was tested using a profilometer (AMBIOS, XP-200) in the range of 3 ± 1 nm to 94 ± 1 nm, and Figure 3a shows that the thickness of the layers increased as the cycle increases. The system layer was coated on the microscope glass slide, and it was attached to the prism using index matching gel. The SPR signal was separately registered for each thickness in the presence of DDW ($n = 1.3323$). Figure 3b,c shows the SPR results to test the refractive index of the layers and baseline. The refractive index of the layer was achieved by analysis of the SPR signal using Fresnel's theory for the multilayer system when the refractive index of the gold layer was $0.237 + 3.335i$.

Fresnel's theory predicts the reflection coefficient (r) from dielectric and metal medium such as the gold layer. The matrix form that was presented in ref. [33,34] is used for the multilayer system. The reflectance (R) is equal to $r \times r$. If the refractive index (n) and accurate thickness (t) of layers are unknown, they can obtain from the minimum root square of the difference between the theory and experimental value of reflectance as follows [26,27]:

$$\Psi = \sum_{\theta} [R_{\text{Theory}}(\theta, n, t) - R_{\text{Exp}}(\theta, n, t)] \quad (2)$$

where R_{Theory} and R_{Exp} are the theoretical and experimental value of reflectance, respectively.

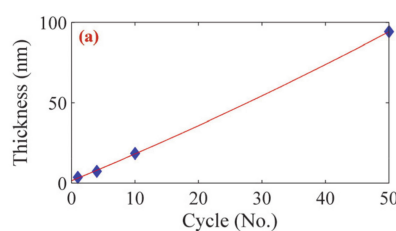


Figure 3. Cont.

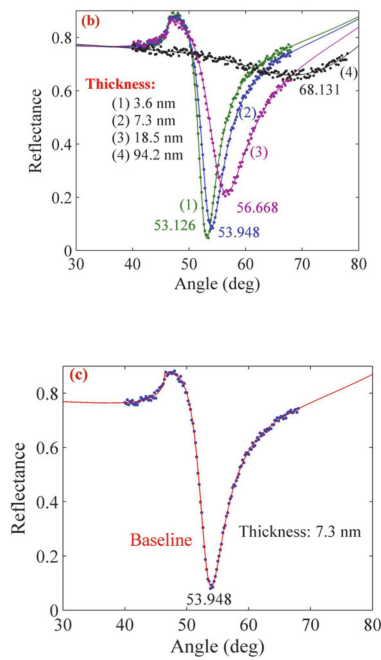


Figure 3. (a) Variation in the thickness of layer with increasing the cycle; (b) The SPR signal related to obtaining the refractive index of the PPy–Chi–BaFe₂O₄ composite layer in the different thickness; (c) The SPR signal at the baseline.

According to the SPR signals analysis, the accurate thickness of layers was in the range of 3.6 nm to 94.2 nm, and the refractive index of the PPy–Chi–BaFe₂O₄ was in the range of 1.67571 + 0.139i to 1.57072 + 0.164i. Figure 3c shows the SPR signal at the baseline when the baseline was obtained at 53.948 using the PPy–Chi–BaFe₂O₄ layer with 7.3 nm of thickness.

The variation of real (*n*) and imaginary (*k*) parts of the refractive index were demonstrated in Figure 4a,b, respectively. Consequently, the real (*n*) part of the refractive index decreased, and the imaginary (*k*) part of the PPy–Chi–BaFe₂O₄ increased when the thickness of the layer increased. The pertinent parameters were listed in Table 1.

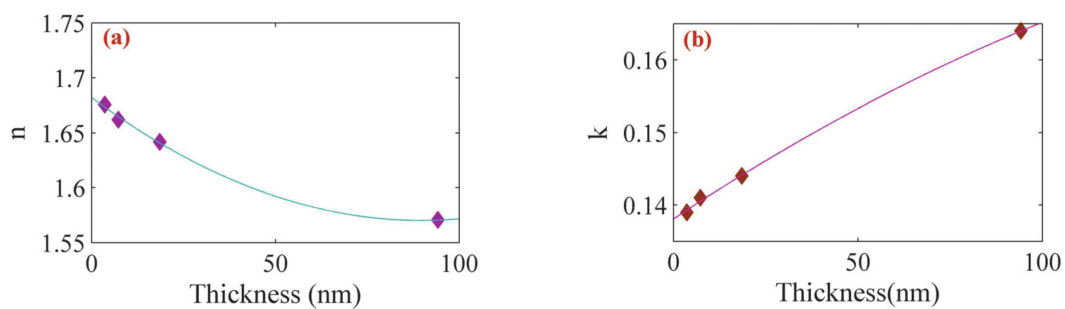


Figure 4. Variation of (a) real (*n*) and (b) imaginary (*k*) parts of the refractive index of PPy–Chi–BaFe₂O₄.

Table 1. The thickness, refractive index, resonance angle, and reflectance of SPR signal related to PPy–Chi–BaFe₂O₄ sensing layer

Sample	Thickness (nm) (Profilometer)	Thickness (nm) (SPR Analysis)	Refractive Index	Resonance Angle	Reflectance
1	3	3.6	1.67571 + 0.139i	53.126°	0.045
2	7	7.3	1.66191 + 0.141i	53.948°	0.088
3	18	18.5	1.64183 + 0.144i	56.668°	0.216
4	94	94.2	1.57072 + 0.164i	68.131°	0.658

The PPy–Chi–BaFe₂O₄ with 7.3 nm thickness was used to measure and detect the low concentration of glucose, sucrose, and fructose. The experiment was separately carried out in the presence of 0.005 ppm (0.0005 mg/dL), 0.05 ppm (0.005 mg/dL), 0.5 ppm (0.05 mg/dL), 5 ppm (0.5 mg/dL), 15 ppm (1.5 mg/dL), and 25 ppm (2.5 mg/dL) of glucose, sucrose, and fructose. The SPR signals were registered, and the variation of resonance angle shift was achieved during 420 s. Figure 5a–c shows the resonance angle shift with time (sensorgram) for the glucose, fructose, and sucrose, respectively. As a result, the experimental values fit well with the first order Langmuir formula ($\Delta\theta = \Delta\theta_{sat}(1 - \exp(-k_a t))$) [35,36].

The concentration of sugars that attached the sensing layer was tested using UV-vis spectroscopy. The PPy–Chi–BaFe₂O₄ sensing layer was separately immersed in the glucose, fructose, and sucrose solutions in the concentration of 15 ppm. The concentrations of glucose, fructose, and sucrose solution were measured before and after the experiment. The degree of adsorption was calculated from [37]:

$$\Pi = 100 \times \frac{C_i - C_f}{C_i} \tag{3}$$

where C_i and C_f were the initial and final concentration of the sugar. Figure 6a1,a2,b1,b2,c1,c2 shows the UV-visible spectra of the glucose, fructose, and sucrose in the concentrations of 2 ppm (0.2 mg/dL), 6 ppm (0.6 mg/dL), 15 ppm (1.5 mg/dL), 20 ppm (2 mg/dL), and 50 ppm (5 mg/dL). The main peak occurred at about 280 nm for them. The intensity peaks were driven for each concentration of the glucose, fructose, and sucrose. Figure 6a3, b3, c3 shows the variation of peak intensity with each concentration of the sugar as a calibration curve. Figure 6a2,b2,c2 show the UV-vis spectra of the sugar solutions after they contacted with the sensing layer and the concentration of glucose, fructose, and sucrose after contact with the PPy–Chi–BaFe₂O₄ sensing layer was achieved from the calibration curve. As a result, the concentration of glucose was lower than that of the other sugars, and it means that the affinity of the PPy–Chi–BaFe₂O₄ nanocomposite layer to the adsorption of the glucose is much higher than that of the other sugars. The concentration value of the sugar and the degree of adsorption are listed in Table 2.

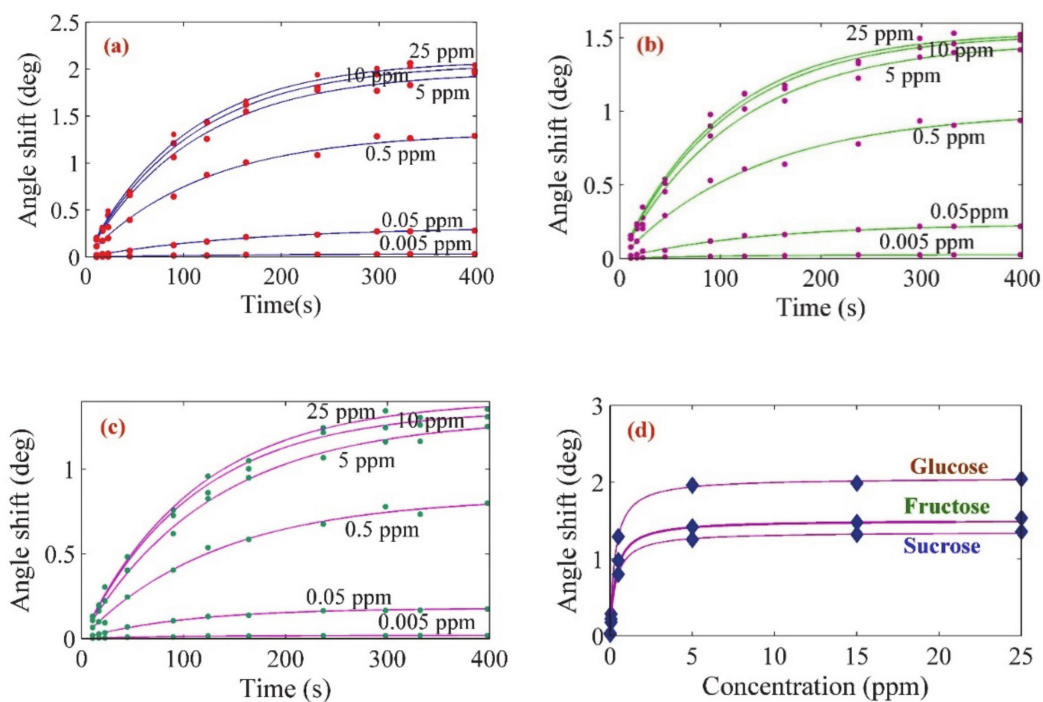


Figure 5. The variation of the resonance angle shift with time-related to (a) glucose, (b) fructose, and (c) sucrose. (d) Variation of the resonance angle shift with the concentration of the sugar.

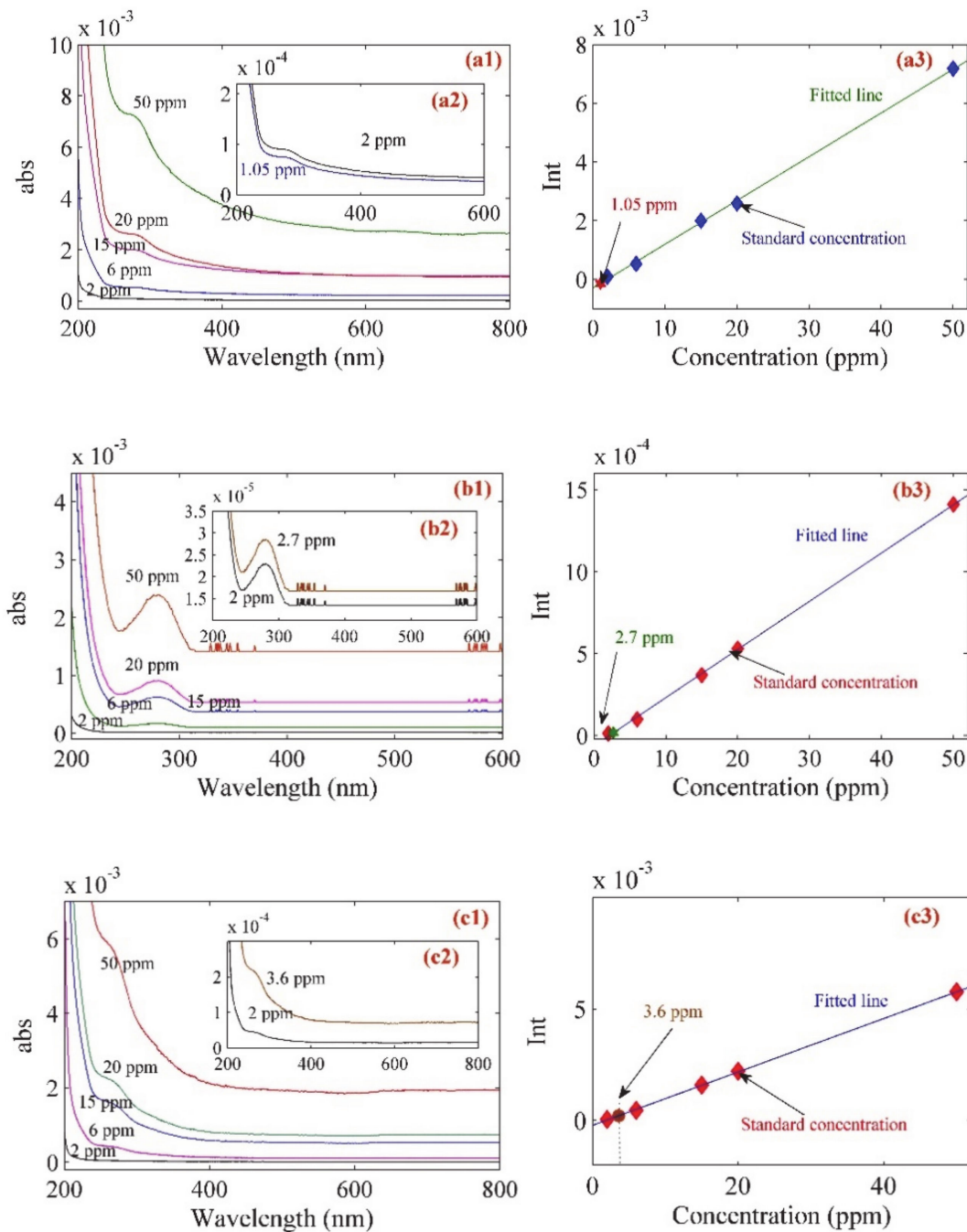


Figure 6. (a1,a2) The UV-vis spectra of the different concentration of glucose (b1,b2) The UV-vis spectra of the different concentration of fructose, (c1,c2) The UV-vis spectra of the different concentrations of sucrose. The calibration curve for (a3) glucose, (b3) fructose, and (c3) sucrose.

Table 2. The concentrations of the sugar before and after adsorption with the sensing layer and the degree of adsorption of the sensing layer.

Sample	C _i (ppm)	C _f (ppm)	Degree of Adsorption (II)
Glucose	15 (1.5 mg/dL)	1.05 (0.105 mg/dL)	93%
Fructose	15 (1.5 mg/dL)	2.7 (0.27 mg/dL)	82%
Sucrose	15 (1.5 mg/dL)	3.6 (0.27 mg/dL)	76%

Magnetic nanoparticles and chitosan can be used for sugar sensor application, because they contribute to transfer the electron between a receptor (sensing layer) and sugar [1,2,16]. The BaFe₂O₄ NPs can enhance the electron transfer between glucose, fructose, and sucrose with the sensing layer. The molecule of glucose contains one hydroxyl group (OH) and one hydroxymethyl group (CH₂OH) at the edge of the molecule plane, and the hydroxyl group can interact with the BaFe₂O₄ -NPs in the sensing layer. The difference between glucose and fructose is in the number of hydroxyl groups at the edge of molecule planes so that fructose contains two hydroxymethyl groups (CH₂OH) at the edge of molecule plane, and they cause the space moment between fructose and BaFe₂O₄ NPs. Moreover, the number of hydroxyl groups (OH) in glucose is higher than those in fructose. Therefore, the tendency of glucose to exchange the electron with a sensing layer is higher than fructose [2,38]. The molecule of sucrose is a combination of glucose and fructose, and it is very heavy and stable. Hence, the tendency of sucrose to exchange the electron with BaFe₂O₄ NPs is very weak. Consequently, the degree of adsorption for glucose is higher than the degree of adsorption of fructose and sucrose. Therefore, the PPy–Chi–BaFe₂O₄ nanocomposite layer is sensitive to bind the low concentration of the glucose.

4. Conclusions

The PPy–Chi–BaFe₂O₄ nanocomposite layer was prepared using electrodeposition technique. The cyclic voltammetry method was used in a different cycle to control the thickness of the layer, which was in the range of 3.6 nm to 94.2 nm. The refractive indices of the PPy–Chi–BaFe₂O₄ composite layers were measured using the SPR method, and they ranged from 1.67571 + 0.139i to 1.57072 + 0.164i, and the resonance angle shifted from 53.126° to 68.131°. The PPy–Chi–BaFe₂O₄ nanocomposite layer was used to detect the sugar. As a result, the affinity of the sensing layer to bind the glucose was higher than that of sucrose and fructose, and the limit sensor was about 0.005 ppm (0.0005 mg/dL). Consequently, PPy–Chi–BaFe₂O₄ nanocomposite layer tends to interact with sugar, and it can adsorb the glucose well.

Author Contributions: A.R.S., P.M.N., M.N., and Y.W.F. S.S.; methodology, A.R.S., M.N., A.M.; software, A.R.S. and Y.W.F., M.N., A.M.; formal analysis, A.R.S., P.M.N.; investigation, A.R.S.; data curation, A.R.S.; writing—original draft preparation, A.R.S., P.M.N., M.N., and A.M., H.M.K.; writing—review and editing, A.R.S.; project administration, A.R.S., S.S.; funding acquisition. All authors have read and agreed to the published version of the manuscript.

Funding: This research was funded by Geran Putra Berimpak, Universiti Putra Malaysia.

Acknowledgments: The authors acknowledge funding from the Universiti Putra Malaysia, under Geran Putra Berimpak (UPM/800-3/31/1GPB/2019/9674700) and the Institute of Advanced Technology (ITMA) UPM to provide the analytical facilities.

Conflicts of Interest: The authors declare no conflict of interest

References

1. Taguchi, M.; Ptitsyn, A.; McLamore, E.S.; Claussen, J.C. 2014 Nanomaterial-mediated Biosensors for Monitoring Glucose. *J. Diabetes Sci. Technol.* **2014**, *8*, 403–411. [[CrossRef](#)] [[PubMed](#)]
2. Su, L.; Feng, J.; Zhou, X.; Ren, C.; Li, H.; Chen, X. Colorimetric Detection of Urine Glucose Based ZnFe₂O₄ Magnetic Nanoparticles. *Anal. Chem.* **2012**, *84*, 5753–5758. [[CrossRef](#)] [[PubMed](#)]
3. Yadava, J.; Rani, A.; Singh, V.; Murari, B.M. Prospects and limitations of non-invasive blood glucose monitoring using near-infrared spectroscopy. *Biomed. Signal Process. Control.* **2015**, *18*, 214–227. [[CrossRef](#)]
4. Pandey, R.; Paidi, S.K.; Valdez, T.A.; Zhang, C.; Spegazzini, N.; Dasari, R.R.; Barman, I. Noninvasive Monitoring of Blood Glucose with Raman Spectroscopy. *Acc. Chem. Res.* **2017**, *50*, 264–272. [[CrossRef](#)]
5. Nor, N.M.; Razak, K.A.; Lockman, Z. Physical and Electrochemical Properties of Iron Oxide Nanoparticles-modified Electrode for Amperometric Glucose Detection. *Electrochim. Acta* **2017**, *248*, 160–168.
6. Wahjudi, P.N.; Patterson, M.E.; Lim, S.; Yee, J.K.; Mao, C.S.; Paul, L. Measurement of Glucose and Fructose in Clinical Samples Using Gas Chromatography/Mass Spectrometry. *Clin. Biochem.* **2010**, *43*, 198–207. [[CrossRef](#)]
7. Damborský, P.; Švitel, J.; Katrlík, J. Optical biosensors. *Essays Biochem.* **2016**, *60*, 91–100.

8. Yeh, Y.-L. Real-time measurement of glucose concentration and average refractive index using a laser interferometer. *Opt. Laser. Eng.* **2008**, *46*, 666–670. [[CrossRef](#)]
9. Yu-Lung, L.; Tsung-Chih, Y.A. Polarimetric glucose sensor using a liquid crystal polarization modulator driven by a sinusoidal signal. *Opt. Commun.* **2006**, *259*, 40–48.
10. Chien, C.; Wen-Chuan, K.; Tung-Sheng, H.; Hui-Kang, T.A. Phase sensitive optical rotation measurement in a scattered chiral medium using a Zeeman laser. *Opt. Commun.* **2004**, *203*, 259–266.
11. Torii, T.; Chiba, H.; Tanabe, T.; Oyama, Y. Measurements of glucose concentration in aqueous solutions using reflected THz radiation for applications to a novel sub-THz radiation non-invasive blood sugar measurement method. *Digit. Health* **2017**, *3*, 1–5. [[CrossRef](#)] [[PubMed](#)]
12. Sadrolhosseini, A.R.; Rashid, S.A.; Jamaludin, N.; Noor, A.S.M.; Isloor, A.M. Surface plasmon resonance sensor using polypyrrole-chitosan/graphene quantum dots layer for detection of sugar. *Mater. Res. Express* **2019**, *6*, 075028. [[CrossRef](#)]
13. Kun Huang, C.; Cheng Chih, H.; Chin, C.D. 2003 Interferometric optical sensor for measuring glucose concentration. *Appl. Opt.* **2003**, *42*, 5774–5776.
14. Kolomenskii, A.A.; Gershon, P.D.; Schuessler, H.A. Sensitivity and detection limit of concentration and adsorption measurements by laser-induced surface plasmon resonance. *Appl. Opt.* **1997**, *36*, 6539–6547. [[CrossRef](#)]
15. Toghiani, K.E.; Compton, R.G. Electrochemical non-enzymatic glucose sensors: A perspective and an evaluation. *Int. J. Electrochem. Sci.* **2010**, *5*, 1246–1301.
16. Amir AL-Mokaram, A.M.A.; Yahya, R.; Abdi, M.; Ekramul Mahmud, H.N.M. One-step electrochemical deposition of Polypyrrole–Chitosan–Iron oxide nanocomposite films for non-enzymatic glucose biosensor. *Mater. Lett.* **2016**, *183*, 90–93. [[CrossRef](#)]
17. Karyakin, A.A.; Vuki, M.; Lukachova, L.V.; Karyakina, E.E.; Orlov, A.V.; Karpachova, G.P.; Wang, J. Processible polyaniline as an advanced potentiometric pH transducer. *Appl. Biosens. Anal. Chem.* **1999**, *71*, 2534–2540. [[CrossRef](#)]
18. Ramanavicius, A.; Kausaite, A.; Ramanaviciene, A.; Acaite, J.; Malinauskas, A. 2006 Redox enzyme–glucose oxidase–initiated synthesis of polypyrrole. *Synth. Met.* **2006**, *156*, 409–413. [[CrossRef](#)]
19. Portaccio, M.; Lepore, M.; Della Ventura, B.; Stoilova, O.; Manolova, N.; Rashkov, I.; Mita, D.G. Fiber-optic glucose biosensor based on glucose oxidase immobilised in a silica gel matrix. *J. Sol-Gel Sci. Technol.* **2009**, *50*, 437–448. [[CrossRef](#)]
20. Salimi, A.; Compton, R.G.; Hallaj, R. Glucose biosensor prepared by glucose oxidase encapsulated sol-gel and carbonnanotube-modified basal plane pyrolytic graphite electrode. *Anal. Biochem.* **2004**, *333*, 49–56. [[CrossRef](#)]
21. Wei, H.; Wang, E. Fe₃O₄ Magnetic Nanoparticles as Peroxidase Mimetics and Their Applications in H₂O₂ and Glucose Detection. *Anal. Chem.* **2008**, *80*, 2250–2254. [[CrossRef](#)] [[PubMed](#)]
22. Naseri, M.; Naderi, E.; Sadrolhosseini, A.R. Effect of Phase Transformation on Physical and Biological Properties of PVA/CaFe₂O₄ Nanocomposite. *Fiber Polym.* **2016**, *17*, 1667–1674. [[CrossRef](#)]
23. Candeia, R.A.; Souza, M.A.F.; Bernardi, M.I.B.; Maestrelli, S.C.; Santos, I.M.G.; Souza, A.G.; Longo, E. Monoferrite BaFe₂O₄ applied as ceramic pigment. *Ceram. Int.* **2007**, *33*, 521–525. [[CrossRef](#)]
24. Sadrolhosseini, A.R.; Naseri, M.; Rashid, S.A. Polypyrrole-chitosan/nickel-ferrite nanoparticle composite layer for detecting heavy metal ions using surface plasmon resonance technique. *Opt. Laser Technol.* **2017**, *93*, 216–223. [[CrossRef](#)]
25. Sadrolhosseini, A.R.; Naseri, M.; Kamari, H.M. Surface plasmon resonance sensor for detecting of arsenic in aqueous solution using polypyrrole-chitosan-cobalt ferrite nanoparticles composite layer. *Opt. Commun.* **2017**, *383*, 132–137. [[CrossRef](#)]
26. Sadrolhosseini, A.R.; Noor, A.S.M.; Maarof, M.M. Application of Surface Plasmon Resonance Based on Metal Nanoparticle. In *Plasmonics—Principles and Applications*; Kim, K.Y., Ed.; IntecOpen: London, UK, 2012; Volume 10, pp. 253–282.
27. Jang, J.; Oh, J.H. Fabrication of a Highly Transparent Conductive Thin Film from Polypyrrole/Poly(methyl methacrylate) Core/Shell Nanospheres. *Adv. Funct. Mater.* **2005**, *15*, 494–502. [[CrossRef](#)]
28. Moozarm Nia, P.; Lorestani, F.; Meng, W.P.; Alias, Y. A novel non-enzymatic H₂O₂ sensor based on polypyrrole nanofibers–silver nanoparticles decorated reduced graphene oxide nano composites. *Appl. Surf. Sci.* **2015**, *332*, 648–656. [[CrossRef](#)]

29. Ruhi, G.; Modi, O.P.; Dhawan, S.K. Chitosan-polypyrrole-SiO₂ composite coatings with advanced anticorrosive properties. *Synth. Met.* **2015**, *200*, 24–39. [[CrossRef](#)]
30. Mandizadeh, S.; Salavati-Niasari, M.; Sadri, M. Hydrothermal synthesis, characterization and magnetic properties of BaFe₂O₄ nanostructure as a photocatalytic oxidative desulfurization of dibenzothiophene. *Sep. Purif. Technol.* **2017**, *175*, 399–405. [[CrossRef](#)]
31. Utami, R.S.; Puspasari, I.; Shyuan, L.K.; Mohamed, A.B.; Alva, S. Effect of Process Parameters on the Synthesis of Polypyrrole by the Taguchi Method. *MJAS* **2016**, *20*, 660–669. [[CrossRef](#)]
32. Moozarm Nia, P.; Meng, W.P.; Alias, Y. One-Step Electrodeposition of Polypyrrole-Copper Nano Particles for H₂O₂ Detection. *J. Electrochem. Soci.* **2016**, *163*, B8–B14.
33. Sharma, K.K. *Optics: Principles and Applications*; Academic Press: CA, USA, 2006; pp. 120–180.
34. Homola, J. *Surface Plasmon Resonance Based Sensors*; Springer: Berlin/Heidelberg, Germany, 2006; pp. 80–110.
35. Beketov, G.V.; Shirshov, Y.M.; Shynkarenko, O.V.; Chegel, V.I. Surface plasmon resonance spectroscopy: Prospects of superstrate refractive index variation for separate extraction of molecular layer parameters. *Sens. Actuators B* **1998**, *48*, 432–438. [[CrossRef](#)]
36. Shishehbore, M.R.; Afkhami, A.; Bagheri, H. Salicylic acid functionalized silica coated magnetite nanoparticles for solid phase extraction and preconcentration of some heavy metal ions from various real samples. *Chem. Cent. J.* **2011**, *5*, 1–10. [[CrossRef](#)] [[PubMed](#)]
37. Sun, M.; Li, P.; Jin, X.; Ju, X.; Yan, W.; Yuan, J.; Xing, C. Heavy metal adsorption onto graphene oxide, amino group on magnetic nanoadsorbents and application for detection of Pb(II) by strip sensor. *Food Agric. Immunol.* **2018**, *29*, 1053–1073. [[CrossRef](#)]
38. Zhang, W.; Li, X.; Zou, R.; Wu, H.; Shi, H.; Yu, S.; Liu, Y. Multifunctional glucose biosensors from Fe₃O₄ nanoparticles modified chitosan/graphene nanocomposites. *Sci. Rep.* **2015**, *5*, 11129. [[CrossRef](#)]



© 2020 by the authors. Licensee MDPI, Basel, Switzerland. This article is an open access article distributed under the terms and conditions of the Creative Commons Attribution (CC BY) license (<http://creativecommons.org/licenses/by/4.0/>).